





Gradient energy-absorbing nature-inspired metamaterial based on the "Schwarz Primitive" geometry

S.V. Balabanov¹ , A.M. Kuropiatnik^{1,2}, M.M. Sychoy^{1,2} , E.A. Pavlova², S.V. Diachenko^{1,2}  

¹National Research Center "Kurchatov Institute", Konstantinov Petersburg Nuclear Physics Institute – Grebenshchikov Institute of Silicate Chemistry, St. Petersburg, Russia

²St. Petersburg State Institute of Technology, St. Petersburg, Russia

svdiachenko@technolog.edu.ru

ABSTRACT

Gradient energy-absorbing nature-inspired cellular metamaterial with high energy-absorbing properties has been developed, made from polyamide-12 using selective laser sintering technology. It is shown that the gradient structure provides the effect of "pseudo-plastic failure" due to layer-by-layer deformation of the metamaterial with a significant increase in the energy absorption value, which was 1.88 MJ/m³ for the plastic series, and 1.45 MJ/m³ for the brittle series.

KEYWORDS

cellular materials • triply periodic minimal surfaces • additive technologies • 3D printing • strength deformation • selective laser sintering • pseudo-plastic failure • gradient cellular structures

Acknowledgements: The work on modeling, manufacturing and research of metamaterials was carried out within the framework of the Russian Science Foundation project "New generation energy-absorbing materials based on gradient cellular structures". (Agreement No. 20-73-10171; available online: <https://www.rscf.ru/project/20-73-10171>). The work on testing and analysis of metamaterials was carried out with financial support within the framework of the State Task No. 1024030700040-3-1.4.3 "Chemistry, physics and biology of nanostates".

Citation: Balabanov SV, Kuropiatnik AM, Sychoy MM, Pavlova EA, Diachenko SV. Gradient energy absorbing nature-inspired metamaterial based on the "Schwarz primitive" geometry. *Materials Physics and Mechanics*. 2025;53(2): 157–167.

http://dx.doi.org/10.18149/MPM.5322025_14

Introduction

Materials with repeating cells of varying shapes and sizes are one of the types of modern metamaterials [1]. Currently, cellular materials find extensive applications across multiple scientific and technical domains: mechanical engineering (energy absorbers, thermal and acoustic insulation substrates [2]), medicine (implants and prostheses), chemical industry (functional reactor and catalyst bases) etc. In nature, cellular materials exist as bionic structures – honeycomb formations of highly organized insects (bees, wasps, hornets), lipid bilayer membranes, marine coral formations, beetle exoskeletons, mammalian bones etc. However, most such structures are either doubly periodic (exhibiting structural periodicity along two directions), like honeycombs, or spatially stochastic (irregular) – e.g., polymer and metal foams.

The works of Academician V.Ya. Shevchenko's team [3–9] have demonstrated that to enhance physical and mechanical properties of cellular materials in technical applications, triply periodic minimal surfaces (TPMS) show particular promise. TPMS are



regular triply periodic structures (periodic along three directions) with zero mean curvature. A surface is considered minimal, when its mean curvature equals zero at any point [10]. It was the German mathematician Karl Schwarz who introduced the TPMS geometry based on mathematical calculations in 1865 [11]. Due to its isotropic cellular structure, large specific surface area, smoothness and controlled geometric parameters (due to the change in the parameters of the mathematical equation describing their geometry), TPMS-based materials offer promising solutions for various physical applications [12–15].

It is known that TPMS-based materials efficiently dissipate various energy types, including mechanical energy [16], and serve as structural materials due to their high specific strength and high isotropy of physical properties [17,18]. It is worth noting that materials with a similar structure are also found in nature – in cuticular structures in butterfly wing scales [19], chloroplast membranes [20], armadillo armor [21], fish scales [22] – qualifying TPMS as nature-inspired structures.

However, their structural complexity long hindered manufacturing TPMS-based materials [23]. Widespread research and practical implementation only became feasible with additive manufacturing (AM) rapid development. Today, AM is a pivotal tool for developing novel promising materials and products for high-tech industries [24]. 3D printing significantly expands production capabilities and is integral to "digital materials science" concept [25]. AM enable creating complex geometries unattainable via traditional subtractive methods of manufacturing [26], particularly TPMS-based cellular materials. Nevertheless, despite active research and popularization, precise methods and approaches to design and prediction of mechanical and other physical properties of TPMS-based cellular materials and similar ones remain underdeveloped due to their topological complexity.

This study aims to develop a gradient cellular material with high energy-absorption capacity and controlled deformation mechanisms. Gradient materials here denote macroporous structures with directional mechanical property variations via geometric modulation. The work comprehensively investigates the physical and mechanical properties of a gradient cellular material with Schwarz Primitive (Schwarz P) geometry, comparing results with similar non-gradient macroporous structures.

Materials and Methods

Manufacturing technology

For the research purposes, 3D models of specimens with Schwarz P surface geometry were developed, described by an implicit function with a varying unit cell size parameter t [16] according to the equation:

$$a \cdot \cos(x) + b \cdot \cos(y) + c \cdot \cos(z) = t. \quad (1)$$

where a , b , c are the numerical coefficients in the equation; t is a geometric parameter (indicator).

The isosurface level parameter t took the following values: -0.9, -0.6, -0.3, 0, 0.3, 0.6. In this case, the numerical coefficients a , b , c were equal to 1. It should be noted that as parameter t increased, the unit cell size in the TPMS structure decreased while maintaining equal values along all three directions (Fig. 1). To study the influence of

structural heterogeneity on the physical and mechanical properties of the specimens, a gradient sample was developed with height-dependent geometric parameter t , where $t = z/24$, with z being the height coordinate.

Modeling was performed using parametric methods in Rhinoceros 6 software with Grasshopper plugin, and the models were saved in STL format for 3D printing. Autodesk Netfabb software was used to correct errors in STL files; structure renders are shown in Fig. 1.

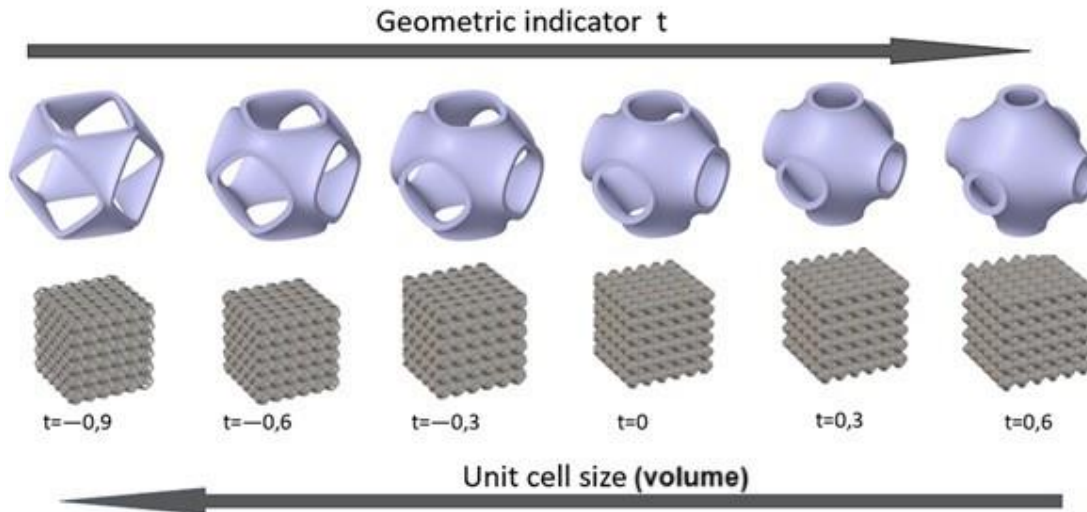


Fig. 1. Renders of the Schwarz P structure with different parameters (geometric indicator t)

The selective laser sintering (SLS) technology was chosen as the 3D printing method, implemented on an FORMIGA P100 3D printer by Electro Optical Systems. In this method, a laser sinters polymer powder particles layer by layer, fusing them together to create the structure [27]. The key advantages of this technology include high printing accuracy and absence of support structures [28]. EOS Parameter Editor software was used to prepare models for printing. Two series of specimens were printed from polyamide-12 (PA-12, $\rho \approx 1 \text{ g/cm}^3$) with dimensions of $60 \times 60 \times 60 \text{ mm}^3$ ($6 \times 6 \times 6$ unit cells) with different t parameter values under varying manufacturing conditions (Table 1).

Table 1. 3D printing modes for PA-12 samples

| No. | Parameter | Mode 1 | Mode 2 |
|-----|------------------------------------------------|--------|--------|
| 1 | Layer thickness h , μm | 100.0 | |
| 2 | Table temperature T_1 , $^{\circ}\text{C}$ | 169.5 | 173.0 |
| 3 | Chamber temperature T_2 , $^{\circ}\text{C}$ | 150.0 | 173.0 |
| 4 | Laser power P , W | 22.0 | |
| 5 | Filling distance s , μm | 250.0 | |
| 6 | Laser scanning speed V , m/s | 25.0 | |
| 7 | Energy density E , J/cm^3 | 35.2 | |

To introduce a gradient of physical and mechanical properties into the base structure, a gradient was applied along one direction (height) by linking it to the TPMS equation. Thus, the equation of the gradient Schwarz P surface, considering Eq. (1), took the form:

$$\cos(x) + \cos(y) + \cos(z) = \frac{z}{24}. \quad (2)$$

It is assumed that the strength of each layer in the gradient structure corresponded to the strength of an isotropic specimen with the same t value. The general appearance of the gradient cellular structure is shown in Fig. 2.

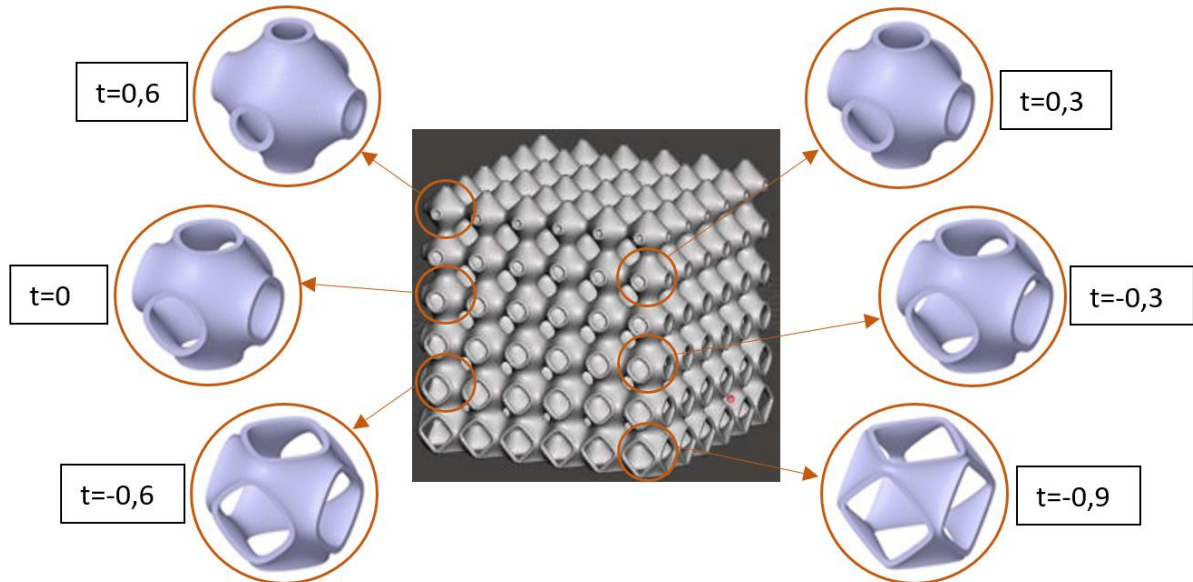


Fig. 2. The general appearance of the gradient cellular structure

Testing

The specimens were subjected to compression testing according to GOST 4651-2014 (ISO 604:2002)¹ standards on a REM-50-A-1-1 tensile testing machine with maximum load capacity of 50 kN and loading rate of 5 mm/min. Given that 3D-printed products exhibit mechanical property anisotropy, compression strength tests were conducted along the specimen's build direction [8]. In addition to TPMS compression tests, tensile tests of witness samples were performed in accordance with GOST 11262-2017 (ISO 527-2:2012)² at 5 mm/min rate to investigate the material's physical and mechanical properties.

Results and Discussion

Non-gradient specimens

The test results yielded stress σ versus relative strain ϵ curves for series 1 and 2 specimens (Figs. 3 and 4). The deformation curves differed significantly: specimens printed at lower temperature (series 1, mode 1) exhibited dominant elastic-plastic deformation up to $\epsilon \approx 70\%$ (Fig. 3(a)), whereas series 2 specimens (Fig. 3(b)) manufactured under mode 2 failed brittly at 15–20 % strain.

¹ Interstate Council for Standardization, Metrology and Certification (ISC). *Plastics. Compression test method*. GOST 4651-2014. 2014. 16 p.

² Interstate Council for Standardization, Metrology and Certification (ISC). *Plastics – Determination of tensile properties – Part 2: Test conditions for moulding and extrusion plastics, MOD*. GOST 11262-2017. 2018. 24 p.

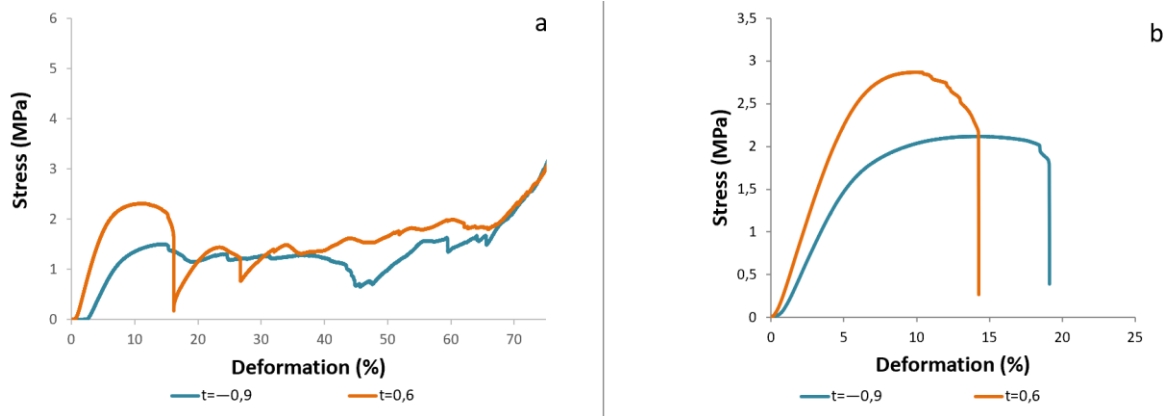


Fig. 3. Deformation curves for both series at different t parameter: (a) series 1; (b) series 2

To evaluate physical and mechanical properties of the samples under study, compression curves were analyzed and witness samples underwent tensile testing. Stress calculation was performed according to the following equation:

$$\sigma = \frac{N}{S}, \quad (3)$$

where N is the applied load and S is the specimen base area (calculated via outer dimensions).

As shown in Fig. 4, the series 1 specimens demonstrate eight distinct characteristic regions. During specimen deformation in region I, stress increases sharply while maintaining proportionality law (Hooke's law), therefore this region can be classified as elastic deformation zone. At the end of region I, the Hooke's law no longer applies. Six subsequent regions (regions II–VII) exhibit elastic-plastic deformation with mutually similar patterns – regions of cellular structure layers deformation. Region II reaches the maximum (ultimate tensile strength) where rapid deformation of the first cellular layer occurs. Stress then decreases with continuing deformation accumulation. At the end of region II and at the beginning of region III, complete "collapse" of the first cellular layer occurs. Regions III–VII qualitatively replicate region II. At the end of region VII and at the beginning of region VIII, the sixth (final) cellular layer "collapse". Region VIII is characterized by exponential load increase, marking the onset of plastic deformation.

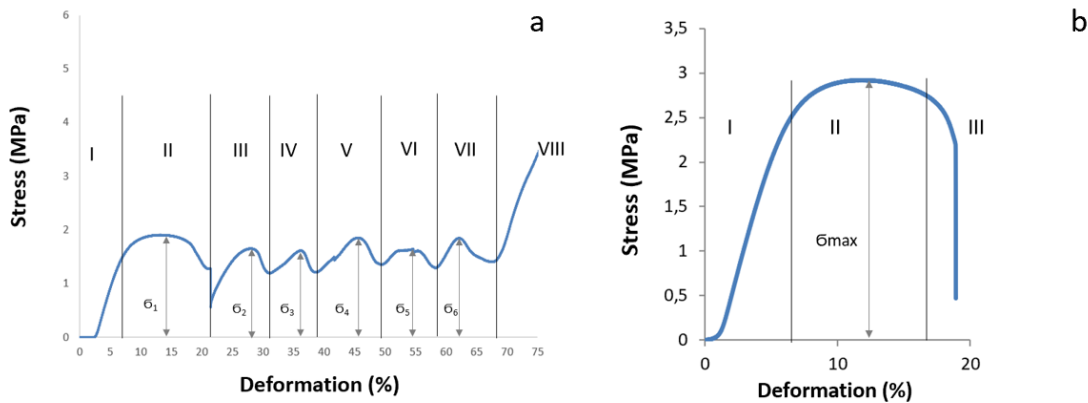


Fig. 4. Deformation curves for both series at $t = 0$: a) series 1; b) series 2

The deformation curve characteristics differ for series 2 specimens. Region I represents the elastic deformation zone, obeying Hooke's law as in Series 1. Region II is the transitional zone where compressive ultimate tensile strength is achieved. Region III shows crack propagation leading to brittle failure of the sample.

Unlike series 1, series 2 specimens exhibit brittle failure – upon reaching ultimate strength, they fracture rather than undergoing progressive layer-by-layer deformation. Comparing Figs. 5(b) and 5(c) one can observe that series 2 specimens fracture similarly to brittle ceramic materials. This behavior is characteristic of brittle materials where failure occurs along planes of maximum shear stress, typically oriented at 45° angles [29].

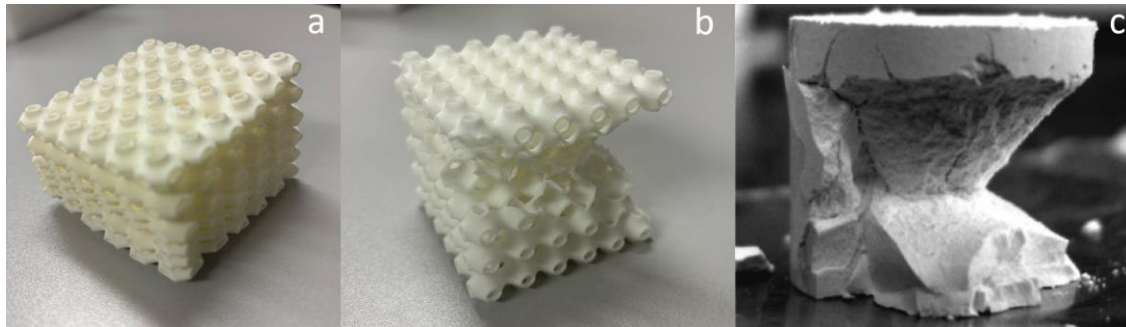


Fig. 5. Post-test specimens: (a) $t = 0.3$, series 1; (b) $t = 0.3$, series 2; (c) ceramic sample

Plasticity of the materials was assessed via indirect metrics: residual relative elongation at rupture δ and residual relative contraction (cross-section reduction) ψ at rupture [9]. Results are summarized in Table 2.

Table 2. PA-12 mechanical properties under tension

| No. | Parameter | Series 1 | Series 2 |
|-----|----------------------------------|----------|----------|
| 1 | σ_{\max} , MPa | 50.0 | 49.0 |
| 2 | $\varepsilon(\sigma_{\max})$, % | 12.9 | 14.6 |
| 3 | ε_{\max} , % | 13.1 | 21.1 |
| 4 | δ , % | 12.9 | 9.8 |
| 5 | ψ , % | 9.3 | 3.0 |
| 6 | E , MPa | 8.3 | 9.5 |

From Table 2, it follows that the change in cross-sectional area ψ and elongation δ for series 1 specimens printed at lower temperature T are higher than for series 2 specimens with increased T . This indicates that series 2 specimens exhibit reduced plastic properties compared to series 1 under equal conditions and identical printing energy density. It is possible that at high sintering temperatures, PA-12 crystallizes, consequently making the printed product more brittle [30]. This leads to the conclusion that to achieve high energy absorption characteristics, it is necessary to consider the polymer's crystallization temperature value, particularly for polyamide, when adjusting printing temperature, as it directly affects the final product's properties.

It is known that energy-absorbing materials should possess high plasticity. Maximum energy absorption A of the specimens was evaluated from the obtained deformation curves using the equation:

$$A = \int_0^{\varepsilon} \sigma d\varepsilon. \quad (4)$$

The test results demonstrate that increasing sintering temperature leads to embrittlement and altered deformation behavior of the specimens (Fig. 3). Consequently, these specimens are unsuitable for mechanical energy absorption applications. Table 3 shows that brittle specimens' energy absorption decreases several-fold compared to the plastic series – for instance, plastic specimens with $t = 0.6$ reach energy absorption of 1.13 MJ/m^3 , while brittle specimens under equal conditions show three times lower values. However, higher sintering temperatures increase specimens' strength and Young's modulus by 1.5 and 2 times, respectively, which is advantageous for their use as structural components.

Table 3 further reveals that increasing t parameter enhances the cellular structure's strength. Additionally, these structures exhibit layer-by-layer deformation and failure. This suggests that creating a gradient structure with varying t parameter between layers would correspondingly increase σ_{\max} progressively from layer to layer.

Table 3. Mechanical properties of two TPMS specimen series

| t | $A, \text{ MJ/m}^3$ | | $\sigma_{\max}, \text{ MPa}$ | | $E, \text{ MPa}$ | |
|------|---------------------|----------|------------------------------|----------|------------------|----------|
| | Series 1 | Series 2 | Series 1 | Series 2 | Series 1 | Series 2 |
| -0.9 | 0.87 | 0.23 | 1.50 | 2.11 | 25.9 | 23.9 |
| -0.6 | 0.77 | 0.32 | 1.64 | 2.83 | 31.8 | 51.6 |
| -0.3 | 0.95 | 0.30 | 1.81 | 2.59 | 38.1 | 50.3 |
| 0.0 | 1.03 | 0.32 | 1.90 | 2.92 | 34.8 | 53.4 |
| 0.3 | 0.99 | 0.39 | 1.94 | 2.83 | 35.5 | 50.2 |
| 0.6 | 1.13 | 0.32 | 2.31 | 2.87 | 46.3 | 52.5 |

Gradient specimen

To improve brittle material's energy absorption, a structure was developed that is capable of sequential layer failure through variation of layers' physical and mechanical properties, achieved by implementing geometric gradient via parameter t modulation. This gradient geometry may compensate for material brittle properties during deformation. Compression tests confirmed that despite inherent brittleness of series 2 specimen, the gradient specimen failed layer-by-layer (Fig. 6), progressing from least robust to most robust layers. During the testing the specimen demonstrated brittle, but local fracture – inside every layer, which led to the effect of "pseudo-plastic behavior" of the specimen.

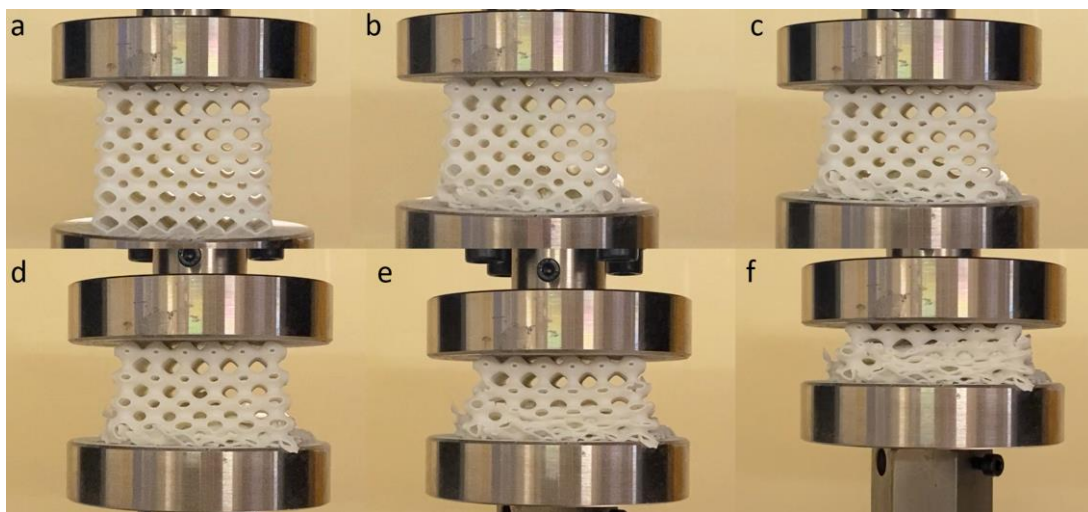


Fig. 6. Sequential layer-by-layer failure of gradient structure (series 2)

For comparison, Fig. 7 presents deformation curves of gradient and isotropic (non-gradient) series 2 specimens with constant t . It is obvious, that the curve characteristics vary, resembling plastic material's deformation curve. Besides, according to the curve characteristics, each layer's strength of gradient structure progressively increases with increasing t value, i.e., the material exhibits spring-like behavior until reaching σ_{\max} , followed by plastic deformation. These results confirm that parameter t variation effectively controls TPMS cellular materials' operational properties.

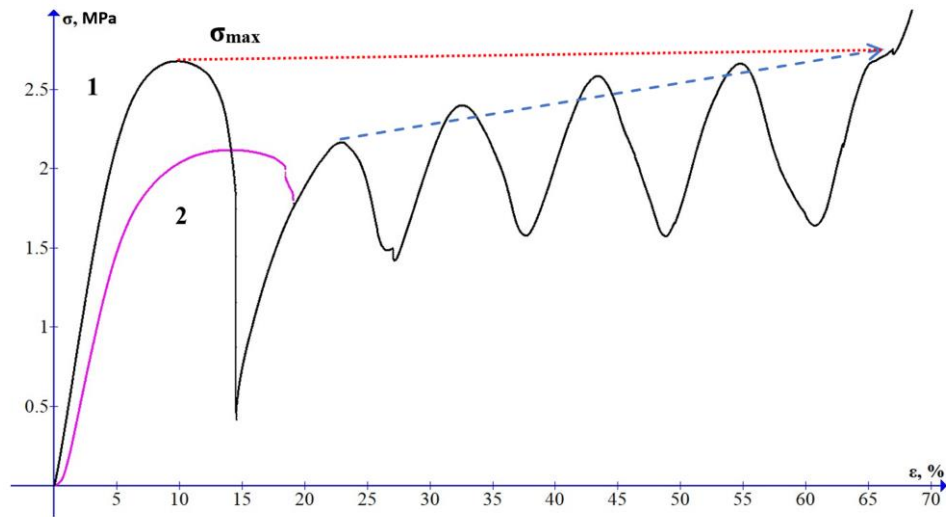


Fig. 7. Deformation curves of cellular structures (series 2, $t = -0.9$):
(1) gradient specimen, (2) isotropic specimen

Figure 8 shows ultimate tensile strength σ_{\max} dependency from the parameter t for both series' gradient specimens. Both series show monotonic ultimate tensile strength increase with increasing t , though brittle series maintains higher absolute values, consistent with non-gradient structures.

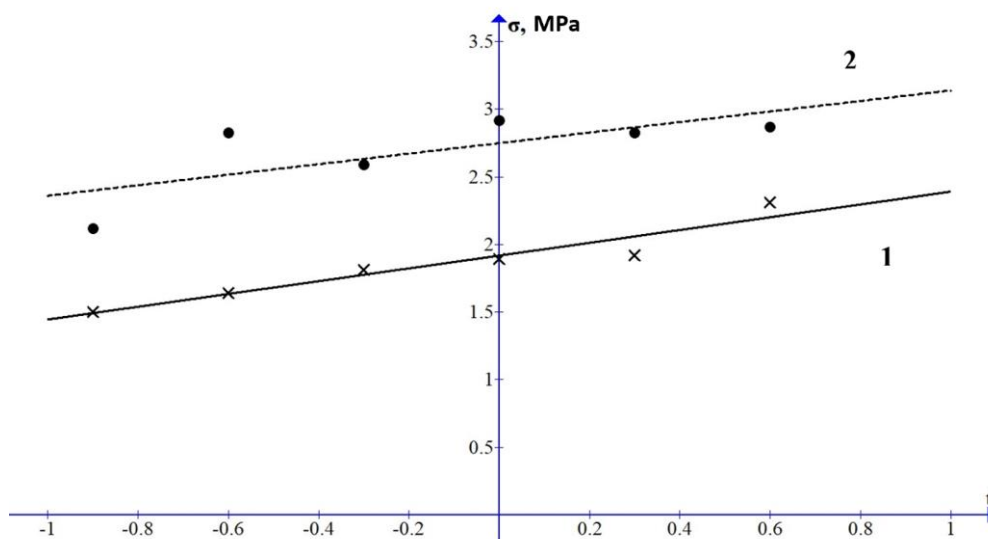


Fig. 8. Ultimate tensile strength σ_{\max} dependency from t parameter for gradient specimens:
(1) series 1; (2) series 2

To use these structures as energy absorbers, energy absorption A_g calculations were carried out for plastic and brittle series, yielding $A_{g1} = 1.88 \text{ MJ/m}^3$ and $A_{g2} = 1.45 \text{ MJ/m}^3$, respectively. According to the results, gradient structures enhanced energy absorption significantly heterogeneity of physical and mechanical properties of the cellular structure layers. When comparing the values of A between gradient and isotropic structures, it can be noted that for the plastic series (1 series) the increase was $\approx 60\%$, while for the brittle series (2 series) the increase was $\approx 270\%$.

Conclusion

Gradient cellular nature-inspired metamaterial samples based on the TPMS "Schwarz Primitive" geometry were developed, fabricated from polyamide-12 using selective laser sintering (SLS) and investigated.

The following tasks were completed:







1. Modeling and manufacturing of a cellular nature-inspired metamaterial with gradient structure.
2. Investigation of mechanical properties of TPMS-based cellular material (Schwarz Primitive) with varying parameter t (cell size).
3. Analysis of mechanical properties of cellular material depending on specimen sintering conditions.
4. Identification of mechanical anisotropy in the gradient structure, mitigating the properties of isotropic TPMS (Schwarz Primitive) made from brittle polyamide.

It was concluded, that increasing t parameter enhances strength and energy absorption, while elastic modulus changes nonlinearly. When changing 3D printing parameters: chamber temperature ($\Delta T_1 = +23.0^\circ\text{C}$) and table temperature ($\Delta T_2 = +3.5^\circ\text{C}$) during sintering, induce brittleness in plastic specimens, likely due to increased crystallinity. Tensile tests revealed reductions in δ (-3.1%) and ψ (-6.3%). For compressed TPMS specimens of two different series with various t values, higher sintering temperatures improve mechanical indicators, such as strength and elastic modulus, but reduce energy absorption.

Gradient structures with varying t parameter along height, printed via mode 2 exhibited a shift in compression failure mechanism: from brittle fracture ($t = \text{const}$) to "pseudo-plastic behavior" ($t = -0.9 \dots 0.6$). They also demonstrated simultaneous improvements in strength and energy absorption. Therefore, it can be concluded, that macrostructural and mechanical property gradient of such specimens effectively counteracts the brittleness of isotropic TPMS, regardless of the base material's plasticity, which is crucial for energy-absorbing applications.

Therefore, it can be said that the study proposes a method for designing macroporous structures that combine high strength and Young's modulus with enhanced energy absorption. High mechanical properties are achieved by optimizing 3D printing parameters to control polymer crystallization during manufacturing process. Decreasing plasticity is compensated by gradient geometry of cellular structure, and energy absorption value is higher than that of non-gradient specimens irrespective of polymer crystallinity.

CRediT authorship contribution statement

Sergey V. Balabanov  : writing – review & editing, writing – original draft; **Artur M. Kuropiatnik**: writing – original draft, investigation; **Maksim M. Sychov**  : supervision, conceptualization; **Emiliya A. Pavlova**: data curation; **Semen V. Diachenko**  : writing – review & editing, data curation.

Conflict of interest

The authors declare that they have no conflict of interest.

References

1. Borovkov AI, Maslov LB, Zhmaylo MA, Tarasenko FD, Nezhinskaya LS. Finite element analysis of elastic properties of metamaterials based on triply periodic minimal surfaces. *Materials Physics and Mechanics*. 2024;52(2): 11–29.
2. Sysoev EI, Sychov MM, Shafigullin LN, Dyachenko SV Design of Sound Absorbing Honeycomb Materials with a Geometry of Triply Periodic Minimal Surfaces (TPMS). *Acoustical Physics*. 2024;70(5): 887–898.
3. Shevchenko V, Balabanov S, Sychov M, Karimova L. Prediction of cellular structures mechanical properties with the geometry of triply periodic minimal surfaces (TPMS). *ACS Omega*. 2023;8(30): 26895–26905.
4. Shevchenko VYa, Sychev MM, Lapshin AE, Lebedev LA, Gruzdkov AA, Glezer AM. Polymer structures with the topology of triply periodic minimal surfaces. *Glass Physics and Chemistry*. 2017;43: 608–610.
5. Arsentev MYu, Sysoev EI, Vorobyov SA, Balabanov SV, Diachenko SV, Sychov MM, Skorb EV Crystal-inspired cellular metamaterials with reduced Poisson's ratio as analogues of TPMS. *Composite Structures*. 2025;363: 119097.
6. Diachenko SV, Dolgin AS, Khristyuk NA, Lebedev LA, Nefedova LA, Pavlov SB, Merenkov KF, Ivkov VI, Dmitrieva AN 3D Printing of Ceramic Elements with Q-Surface Geometry for the Fabrication of Protective Barrier. *Ceramics*. 2023;6(2): 912–921.
7. Dolgin AS, Sychev MM, Bogdanov SP, Khristyuk NA, Kozlov VV Comparative Analysis of Triply Periodic Minimal Surface Corundum Products Obtained by 3D Printing. *Glass Physics and Chemistry*. 2019;45(6): 545–550.
8. Arsentev MYu, Balabanov SV, Makogon AI, Sychev MM. Experimental and theoretical studies of the mechanical properties of 3D printed polyamide products of the Schwarz Primitive topology. *Glass Physics and Chemistry*. 2019;45: 599–602.
9. Arsentev MYu, Sysoev EI, Makogon AI, Balabanov SV, Sychev MM, Hammouri MH, Moshnikov VA. High-throughput screening of 3D-printed architected materials inspired by crystal lattices: Procedure, challenges, and mechanical properties. *ACS Omega*. 2023;8(28): 24865–24874.
10. Lord EA, Mackay AL, Ranganathan S. *New geometries for new materials*. Cambridge, UK: Cambridge University Press: 2006.
11. Yan K, Wang J, Li L, Deng H. Numerical investigation into thermo-hydraulic characteristics and mixing performance of triply periodic minimal surface-structured heat exchangers. *Applied Thermal Engineering*. 2023;230(B): 120748.
12. Fu J, Sun P, Du Y, Li H, Zhou X, Tian Q. Isotropic design and mechanical characterization of TPMS-based hollow cellular structures. *Composite Structures*. 2021;279: 114818.
13. Gado MG, Al-Ketan O, Aziz M, Al-Rub RA, Ookawara S. Triply periodic minimal surface structures: Design, fabrication, 3D printing techniques, state-of-the-art studies, and prospective thermal applications for efficient energy utilization. *Energy Technology*. 2024;12(5): 2301287.
14. Zhang D, Yang Y, Lv X, Rao W-F. Fabrication of piezoelectric structures with high porosity by digital light processing. *3D Printing and Additive Manufacturing*. 2024;11(5): e1877–e1886.
15. Hu Y, Guo Z, Ragonese A. A 3D-printed molecular ferroelectric metamaterial. *Proceedings of the National Academy of Sciences USA*. 2020;117(44): 27204–27210.
16. Feng J, Fu J, Yao X, He Y. Triply periodic minimal surface (TPMS) porous structures: from multi-scale design, precise additive manufacturing to multidisciplinary applications. *International Journal of Extreme Manufacturing*. 2022;4: 022001.
17. Balabanov S, Sychov M, Koshevaya K, Makogon A, Gravit M. Study of isotropy of mechanical properties of the TPMS-based cellular structures. *E3S Web of Conferences*. 2022;363: 04053.

18. Balabanov SV, Makogon AI, Sychoy MM, Gravit MV, Kurakin MK. Mechanical properties of 3D printed cellular structures with topology of triply periodic minimal surfaces. *Materials Today: Proceedings*. 2020;30(3): 439–442.
19. Michielsen K, Stavenga DG. Gyroid cuticular structures in butterfly wing scales: biological photonic crystals. *Journal of the Royal Society Interface*. 2007;5(18): 85–94.
20. Zhan T, Lv W, Deng Y. Multilayer gyroid cubic membrane organization in green alga *Zygnema*. *Protoplasma*. 2017;254: 1923–1930.
21. Chen I, Kiang JH, Correa V, Lopez MI, Chen P-Y, McKittrick J, Meyers MA. Armadillo armor: Mechanical testing and micro-structural evaluation. *Journal of the Mechanical Behavior of Biomedical Materials*. 2011;4(5): 713–722.
22. Rawat P, Zhu D, Rahman MZ, Barthelat F. Structural and mechanical properties of fish scales for the bio-inspired design of flexible body armors: A review. *Acta Biomaterialia*. 2021;121: 41–67.
23. Jones A, Leary M, Bateman S, Easton M. Parametric design and evaluation of TPMS-like cellular solids. *Materials & Design*. 2022;221(2): 110908.
24. Jandyal A, Chaturvedi I, Wazir I, Raina A, Ul Haq MI. 3D printing – A review of processes, materials and applications in industry 4.0. *Sustainable Operations and Computers*. 2022;3: 33–42.
25. Bolmaro RE, Brokmeier H-G, Ferrante M, Fourty A, Lins JFC, Malarria J, Martino R, Sandim HRZ, Signorelli JW, Sobrero C, Sordi V. Digital materials science: Why do we need more images and numbers? *Acta Microscopica*. 2009;18(C): 23–24.
26. Gardan J. Additive manufacturing technologies: State of the art and trends. *International Journal of Production Research*. 2016;54: 3118–3132.
27. Fina F, Goyanes A, Gaisford S, Basit AW. Selective laser sintering (SLS) 3D printing of medicines. *International Journal of Pharmaceutics*. 2017;529(1–2): 285–293.
28. Matuš M, Bechný V, Joch R, Drbůl M, Holubják J, Czán A, Novák M, Šajgalík M. Geometric accuracy of components manufactured by SLS technology regarding the orientation of the model during 3D printing. *Manufacturing Technology*. 2023;23(2): 233–240.
29. Savchenko NL, Sevostyanova IN, Sablina TYu, Molnár L, Géber R, Gömze LA, Kulkov SN, Gömze LN. The influence of porosity on the elasticity and strength of alumina ceramics. *Journal of Silicate Based and Composite Materials*. 2014;66(2): 44–47.
30. Dupin S, Lame O, Barrès C, Charneau J-Y. Microstructural origin of physical and mechanical properties of polyamide 12 processed by laser sintering. *European Polymer Journal*. 2012;48(9): 1611–1621.